Composites

CrossMark

Fabrication and characterization of cellulose nanofibrils/epoxy nanocomposite foam

Jinghao Li[1,2], Liqing Wei[2], Weiqi Leng[2], John F. Hunt[2,*], and Zhiyong Cai[2,*]

[1] Department of Biomaterials, International Center for Bamboo and Rattan, Beijing, China
[2] Forest Products Laboratory, USDA Forest Service, Madison, WI 53726, USA

ABSTRACT

Plant-derived cellulose nanofibrils (CNFs) have shown reinforcing effects in polymer nanocomposites. However, freeze-dried CNFs are foam-like material, namely aerogel, that are challenging to disperse in a polymer matrix. In this work, a liquid infusion process was developed for a CNF/epoxy nanocomposite cross-linked foam structure with alterable properties without damaging the foam structure. Microstructures of CNF/epoxy composite foams with different formulations were evaluated using a scanning electron microscope. Surface morphology showed that the CNF cross-linked fibers were well attached by epoxy resin. All absolute and specific mechanical properties [by normalizing the measured parameters against the measured density (ρ)] were investigated. Water resistance and thermal stability of CNF/epoxy composite foams were investigated by water absorption test and thermogravimetric analysis. The concentration of epoxy solution in both tetrahydrofuran (THF) solvents and ethyl acetate (EA) solvents was shown to improve compressive properties and water resistance. The samples fabricated with higher epoxy concentration had higher compressive properties, better water resistance, and better thermal stability. The CNF/epoxy composite foams exhibited compressive modulus and compressive strength up to 175 and 10 MPa, respectively. The water diffusion coefficient of CNF/epoxy composite foams was reduced with an increase in epoxy loading. Further, the CNF/epoxy nanocomposite foams fabricated by the epoxy/THF solution had a more uniform structure and better strength performance than foams fabricated by the epoxy/EA solution, due to the increased solubility of the epoxy in THF compared to epoxy in EA. The glass transition temperature (T_g) was determined by differential scanning calorimetry. The T_g of the nanocomposites was influenced by the CNF/epoxy composition. Therefore, the properties of CNF/epoxy nanocomposite foams can be optimized via changing the solvent and concentration of epoxy resin in solvent.

Address correspondence to E-mail: jfhunt@fs.fed.us; zcai@fs.fed.us

Springer

Introduction

Biopolymer composites are widely used in many engineering applications such as aerospace, packaging, automotive, and construction [1]. Cellulose is one of the most abundant biopolymers on earth, with production levels around 1.5×10^{12} tons each year. Thus, there is an enormous amount of a renewable and biodegradable resource for raw materials [2]. Cellulose fibers are widely recognized for their applicability in environmental-friendly composite materials, but remain a challenge for load-bearing engineering applications to unlock their full potential [3]. Cellulose nanofibrils (CNFs) are one class of natural fibers that have shown remarkable mechanical properties [4]. Recently, the utilization of CNFs for light-weight nanocomposites has attracted considerable attention [5]. When cellulose was reduced from bulk wood cells to nanofibrils, the elastic modulus increased from about 10 to 70 GPa [6], which provided an opportunity to develop a new generation of eco-friendly composite materials [7]. The CNFs can be used to produce either films or sponges for different applications such as oil remover, water filter, air filter, nanogenerator, substrate, and other uses [8–12]. Recently, CNFs were used to make aerogel for mechanical applications [11, 13]; however, the high water solubility, low durability, and low compressive properties are still barriers for full implementation for many engineering applications.

Aerogels with porous structure are considered lightweight solid materials prepared by removing liquid solvent from the hydrogel and exhibit many promising properties such as high porosity, ultralow density, high surface area, and low thermal conductivity [11]. These promising properties allow aerogels to be used in many applications such as catalysts, thermal insulation, and filtration [14–16]. Recently, bio-based aerogels have attracted a significant amount of attention. Self-assembled CNF is an attractive biopolymer for the production of bio-based aerogels due to its biodegradability, biocompatibility, availability, and renewability. The high surface area of CNF makes it a good candidate for the production of aerogels. The CNF aerogels are ultra-lightweight materials that can be formed by the removal of water from a gel without collapsing the network structure. The most common procedures used to form aerogels include supercritical carbon dioxide drying, freeze-casting, and vacuum-drying, where CNF aerogels can be functionalized for different applications such as superabsorbent, supercapacitor and photoanode materials [17–19]. Because of its ultra-lightweight characteristics and micro-porous structure, it also has potential as an eco-friendly alternative to replace traditional polyurethane structural foam for some engineering applications. However, the low relative strength and high water solubility of pure CNF aerogel are still obstacles when competing with current foam.

Epoxy has many good qualities as a structural resin where high strength, good stability, and wide compatibility are often used in engineering applications [20–25]. Epoxy resin may be an ideal material for possible development of a new CNF/epoxy nanocomposite foam for building and structural insulation material. However, most epoxy resins have high viscosity that causes low fluidity thus preventing penetration into the micro-porous CNF aerogel.

In this study, a new fabrication process was developed to produce CNF/epoxy nanocomposite foams; various strength and performance characteristics of CNF/epoxy nanocomposite foams can be achieved using different formulations. These composite foams were created by infusing diluted epoxy in tetrahydrofuran (THF) or ethyl acetate (EA) solvent into the CNF aerogel for potential use in structural materials. The morphology, crystalline structure, and thermos-physical properties of the new CNF/epoxy nanocomposite foams were evaluated using scanning electron microscope (SEM), water absorption test, thermogravimetric analysis (TGA), compression test, differential scanning calorimetry (DSC), and X-ray diffraction (XRD).

Materials and methods

Materials

TEMPO-oxidized CNFs suspension (0.9 wt%) was used in this experiment that was produced by USDA Forest Service Forest Products Laboratory pilot plant (Madison, WI, US). Details of the manufacturing process are described elsewhere [26, 27]. Epoxy resin 635 with a density of 1110 kg/m^3 was obtained from US Composites Inc. (West Palm Beach, FL, US). This 3:1 ratio epoxy with medium hardener has a 8–10 h

cure time at room temperature. THF and EA were both procured from Sigma-Aldrich Co. LLC (St. Louis, MO, USA).

Experiments and preparation of CNF/epoxy nanocomposite foam

Figure 1 illustrates the fabrication processes of CNF/epoxy nanocomposite foam. The 0.9% TEMPO-oxidized CNFs suspension was frozen by liquid nitrogen/ethanol solution, followed by freeze-drying process using Labconco system (Kansas City, MO, USA) under a vacuum of 0.01 MPa with cooling coil temperature of -105 °C for 3 days to obtain the CNF aerogel. Epoxy resin was dissolved in solvent (EA and THF) to obtain an epoxy solution with a range of concentrations (10, 20, 30, and 40 vol%). The CNF aerogel was immersed in the epoxy solution under vacuum. It was observed that the epoxy/solvent solution exhibited low fluidity when the epoxy

concentrations were over 40 vol%, so the concentration over 40 vol% was not considered in this study.

After the CNF aerogel was completely saturated, the uncured CNF/epoxy aerogel was placed in the oven at 70 °C for 4 h until the solvent volatilized and epoxy cured. The thermal cross-linking was accomplished by the epoxy resin. Formulation and sample codes are shown in Table 1. Nanocomposite density was estimated based on the initial conditioned dry weight and dimensions (five replicates).

Morphology

CNF aerogel, neat epoxy resin, and nanocomposite samples were all cryosectioned by first freezing the sample with liquid nitrogen, then using a razor blade to cut in the radial cross-sections (at right angle to axis) and the longitudinal sections (through the axis) of the bulk sample. The purpose was to observe internal surface morphologies. Samples were mounted with conductive carbon tape, sputter coated with gold and imaged using field emission scanning electron microscope (Zeiss Leo 1530) at a 5 mm working distance and a 5 kV accelerating voltage.

Compression test

The compression test was performed on CNF/epoxy nanocomposite foams according to ASTM D695-15 [28]. The dimension of samples was 12.5 mm × 12.5 mm × 6.4 mm. All the samples were conditioned at 23 °C and 65% RH for 2 weeks before tests. Five replicates were tested for each formulation. The compressive strength and elastic modulus were reported. All specific properties were calculated by
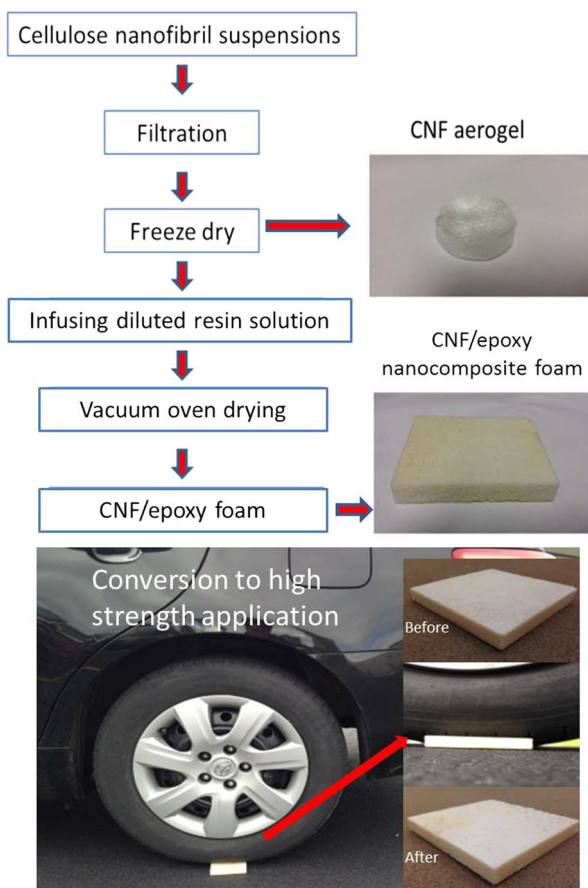

Figure 1 Schematic illustration of the fabrication process of CNF/epoxy nanocomposite.

Table 1 Preparation and formulas of CNF/epoxy nanocomposite foams

Sample	Solvent	Epoxy concentration in solvent (vol%)
CNF	–	0
CNF/EPT10	THF	10
CNF/EPT20	THF	20
CNF/EPT30	THF	30
CNF/EPT40	THF	40
CNF/EPE10	EA	10
CNF/EPE20	EA	20
CNF/EPE30	EA	30
CNF/EPE40	EA	40

normalizing the measured strength and modulus against the measured density (ρ, kg/m^3) of each sample type [29].

Water absorption test

The conditioned samples were weighed and then immersed in distilled water. Samples were removed after 20 min and left to drip any free water for 2 min before weighing. This process was performed every 20 min until the data trend stabilized, and then the measurement was performed at 4 h increments over a span of 24 h. The water absorption was calculated according to the formula, Eq. 1 (ASTM D570-98) [30]:

$$\text{Water absorption}\,(\%) = \frac{W_t - W_0}{W_0} \times 100\% \qquad (1)$$

where W_t and W_0 denote the weight of sample after and before the water absorption test.

The water diffusion coefficient (D_f) of CNF/epoxy samples was calculated using Eq. (2) [31]:

$$D_f = \pi(h/(4M_\infty))^2 \left(\Delta M/\Delta t^{\frac{1}{2}}\right)^2 \qquad (2)$$

where M_∞ is the maximum MC measured at the end of the test, h is the sample thickness corresponding to M_∞, t is time, and $\Delta M/\Delta t^{\frac{1}{2}}$ is the initial slope from the MC versus $t^{1/2}$ relation.

Thermal stability test

Thermal stability of neat CNF, epoxy, and nanocomposites were assessed by TGA (PerkinElmer Pyris 1). Samples (3–5 mg) were heated from 50 to 650 °C with a ramp rate of 10 °C/min under a flowing nitrogen atmosphere (20 mL/min).

Wide angle X-ray diffraction (XRD) measurement

The X-ray diffraction (XRD) patterns were obtained with a Bruker Discovery 8 diffractometer using Cu Kα rotation tube at 50 kV and 1000 μA with scanning over the range of $2\theta = 5°–60°$.

Thermal analysis (DSC)

Differential scanning calorimetry (DSC) was performed on neat epoxy and nanocomposite samples (5 mg) using a TA instrument model Q2000 DSC with refrigerated cooling. The samples were firstly

equilibrated at -50 °C for 3 min then ramped to 160 °C at 10 °C/min. Data were analyzed using TA Universal Analysis v4.5A software. The glass transition temperature (T_g) was determined from the heating scan curve.

Results and discussion

Morphology

Figure 2 shows the morphologies of pure CNF aerogel and neat cured epoxy resin. The flake-like (or sheet-like) CNF walls with cross-linked structure were observed in the pure CNF aerogel sample (Fig. 2a). Compared with CNF aerogel, the neat epoxy resin was cured under room temperature resulting with a solid and smooth structure, as shown in Fig. 2b. Figure 3 shows the CNF/EPT and CNF/EPE nanocomposite foam. Porous microstructures were observed for CNF/epoxy nanocomposites fabricated with both THF and EA solutions. Compared to pure CNF aerogel with wrinkled flake-like wall microstructure (Fig. 2a), the surfaces of nanocomposites prepared from low epoxy/solvent concentration, i.e., CNF/EPT10, CNF/EPT20, CNF/EPE10, and CNF/EPE20, were smoother (Fig. 3a, b, e, f). This suggested that the CNF aerogel was more readily saturated by the low epoxy concentration solutions in both THF (CNF/EPT) and EA (CNF/EPE). It can be seen in Figs. 2a, 3a, e that the sizes of CNF walls were larger as compared to unfilled CNF aerogels, which was likely caused by swelling of CNF in the solvent bath along with the epoxy curing and solvent volatilizing process. The swollen CNF flake-like micro-wall may have provided better compressive properties, which will be discussed later. For both CNF/EPT and CNF/EPE samples, more epoxy resin was observed on the surfaces with the increase in epoxy content in solution. When the epoxy vol% was increased to 40% (CNF/EPE40 and CNF/EPT40), the CNF aerogels were almost fully covered by the epoxy resin (Fig. 3d, h). Compared with CNF/EPE40, the surface of CNF/EPT40 appears denser and shows a more uniform distribution of epoxy with small epoxy particles. This likely contributed to the better solubility and dispersion of epoxy resin in THF than in EA. The average pore size of pure CNF aerogel was 40 μm, which was slightly higher than similar aerogel prepared by the fast freezing process in the literature
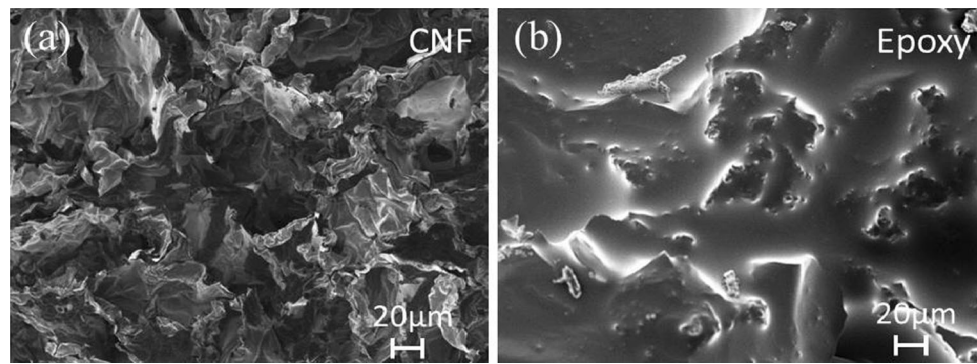
Figure 2 SEM micrographs of CNF and neat cured epoxy: **a** CNF; **b** epoxy.
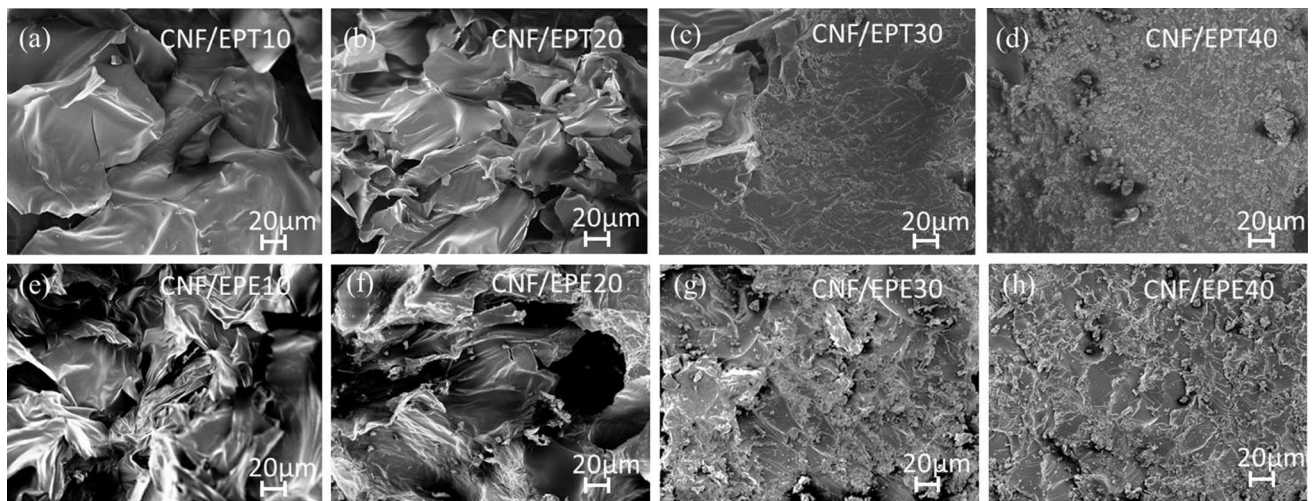

Figure 3 SEM micrographs of CNF/EPT and CNF/EPE nanocomposite foams with 10, 20, 30, and 40% solvent: **a** CNF/EPT10; **b** CNF/EPT20; **c** CNF/EPT30; **d** CNF/EPT40; **e** CNF/EPE10; **f** CNF/EPE20; **g** CNF/EPE30; **h** CNF/EPE40.

[32]. The process and freezing temperature were the primary factors for the pore size. It was also observed that the epoxy filled in the CNF aerogel reduced the average pore size.

Mechanical properties

Light-weight CNF/epoxy nanocomposite foams might potentially be used for compressive components in engineering applications. In order to understand their compressive properties, compression tests were performed on the CNF/epoxy nanocomposite foams. The calculated density, compressive modulus, compressive strength of CNF aerogel, and CNF/epoxy composite foams are shown in Table 2. CNF aerogel exhibited an ultra-light weight with density of 13.03 kg/m^3, which was significantly lower than CNF/epoxy nanocomposites. By soaking CNF aerogel into either epoxy/THF solvent or epoxy/EA solution, the densities of nanocomposites were increased with an increase in epoxy volume percent from 10 to 40%. Furthermore, densities of CNF/EPT40 and CNF/EPA40 significantly increased compared with other CNF/epoxy samples. The density of CNF/EPT10 and CNF/EPT20 had no significant differences compared with CNF/EPA10 and CNF/EPA20. In addition, the trend of densities also increased with increasing epoxy volume content from 10 to 40% with the THF solvent being higher than that corresponding with epoxy/EA solutions. This could be caused by the lower boiling point of THF solvent (66 °C) than for EA solvent (77.1 °C), and hence, the THF can be evaporated from epoxy/THF system more effectively at 70 °C in the oven. In addition, greater solubility of epoxy resin in THF could be the major contributing factor. These findings agree well with the morphological results.

Table 2 Density, compressive modulus, and compressive stress (mean $\pm$ SE) with different epoxy concentrations

Sample	Density ρ (kg/m^3)	Compressive modulus (E, MPa)	Compressive stress (σ, MPa)
CNF	13.03 $\pm$ 0.71[a]	0.083 $\pm$ 0.027[a]	0.011 $\pm$ 0.00029[a]
CNF/EPT10	115.20 $\pm$ 0.75[b]	4.01 $\pm$ 1.00[ab]	0.31 $\pm$ 0.027[ab]
CNF/EPT20	207.16 $\pm$ 7.81[c]	13.10 $\pm$ 2.72[abc]	0.94 $\pm$ 0.11[abc]
CNF/EPT30	349.28 $\pm$ 5.05[d]	53.07 $\pm$ 18.15[d]	3.07 $\pm$ 0.78[d]
CNF/EPT40	756.92 $\pm$ 6.72[e]	174.60 $\pm$ 6.94[e]	9.56 $\pm$ 0.33[e]
CNF/EPE10	84.64 $\pm$ 2.58[bf]	3.13 $\pm$ 0.29[abcf]	0.29 $\pm$ 0.021[abcf]
CNF/EPE20	179.05 $\pm$ 9.53[bcg]	5.40 $\pm$ 1.67[abcfg]	0.83 $\pm$ 0.13[abcfg]
CNF/EPE30	264.09 $\pm$ 4.56[ch]	15.25 $\pm$ 1.43[abcfgh]	1.69 $\pm$ 0.058[cgh]
CNF/EPE40	457.24 $\pm$ 4.20[i]	163.73 $\pm$ 13.57[ei]	7.02 $\pm$ 0.12[i]

[a–i]Letters for statistics, properties with the same letter are not significantly different at 95% confidence interval of probability using Tukey tests

For the compressive modulus and strength, values increased with increasing epoxy concentrations in both THF and EA, as shown in Table 2. Noticeably, the compressive modulus and strength for CNF/EPT40 and CNF/EPT40 were 174.60 and 163.73, and 9.56 and 7.02 MPa, respectively, which were significantly higher than other samples fabricated with lower epoxy volume concentrations. These values were due to the 40 vol% epoxy diluted in solvent which was infused into CNF aerogel porous structures.

The ρ changes with the addition of epoxy were statistically significant at $P < 0.05$ (Table 2), especially for CNF/EPT systems. By normalizing compressive properties against the density, values obtained can be compared to other CNF-based composites. The plot of specific compressive properties is shown in Fig. 4. The pure CNF aerogel shows very low E/ρ (0.006 MPa) and σ/ρ (0.008 MPa) as compared with other CNF/epoxy nanocomposites. With the increase in epoxy loading from 10 to 40%, both the E/ρ and σ/ρ of CNF/epoxy nanocomposite foams fabricated by both epoxy/THF and epoxy/EA increased. Notably, the E/ρ and σ/ρ of CNF/EPT increased by 265 and 178% when the vol% of epoxy with THF increased from 20 to 40%. Similarly, the E/ρ and σ/ρ for CNF/EPE increased by 482 and 141% when the vol% of epoxy in EA increased from 30 to 40%. It was shown that the specific compressive properties of CNF/EP nanocomposite foams increased when the epoxy concentration increased for both THF and EA solvent. For CNF/EP samples at the same level of epoxy concentration fabricated with either THF or EA, the density and compressive properties of CNF/EPT were higher than the results

of CNF/EPE. It is interesting to note that the properties of the sample at 40% epoxy concentration fabricated by EA solvent significantly increased. It is possible that more epoxy was infused into CNF aerogel that resulted in increased specific properties while the sample with 40% epoxy concentration fabricated by THF solvent had higher density and thus lower specific properties. More investigation needs to be done in this area. It is possible that the THF solvent evaporated prematurely during the curing process. The samples were cured in the oven set at 70 °C, because the boiling point for THF is 66.0 °C. While the EA solvent which has a boiling point of 77.1 °C may not have evaporated as quickly as THF solvent. The slower evaporation process for epoxy/EA solution may have influenced the curing process and compressive properties.

Thermal properties

TGA data for CNF, neat cured epoxy, and their CNF/epoxy nanocomposite foams are shown in Fig. 5. The pure CNF showed a slight weight loss at low-temperature range from 100 to 125 °C in terms of evaporation of absorbed and intermolecular H-bonded water [31, 33]. The thermal degradation of pure CNF aerogel occurred at around 215 °C in a nitrogen atmosphere, same as presented in the literature [34], and the entire pyrolysis of pure CNF aerogel was done between 180 and 375 °C. The amount of char residue for pure CNF aerogel was 25.7% at 650 °C. For the neat epoxy resin, the mass loss displayed only one major distinctive stage between 350 and 650 °C. Compared with CNF aerogel and neat epoxy resin, the CNF/epoxy nanocomposite foam had higher

Figure 4 Specific compressive properties: E/ρ and σ/ρ.
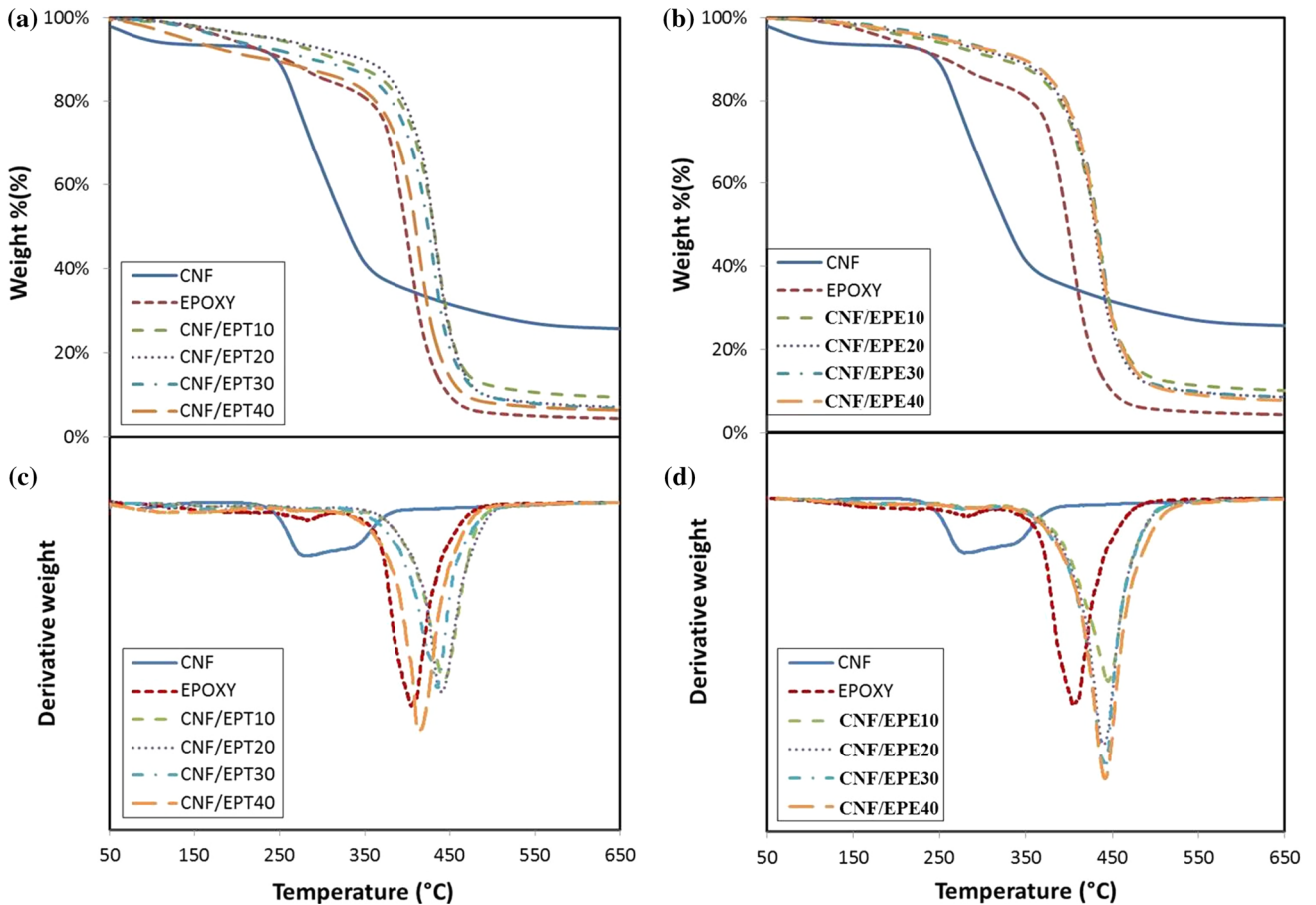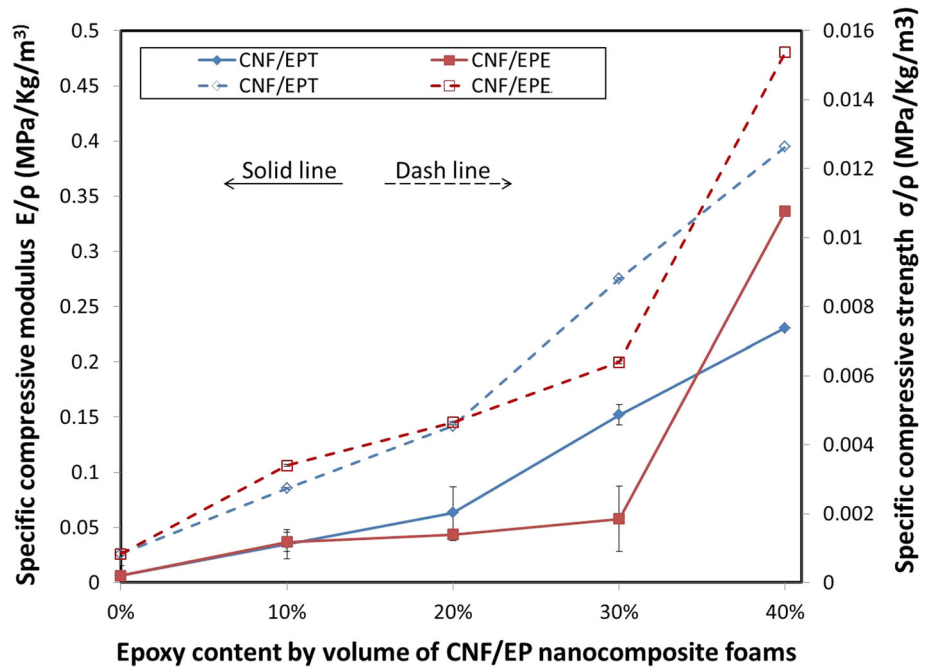

Figure 5 TGA for CNF, epoxy, CNF/EPT, and CNF/EPE **a** and **c** weight loss; **b** and **d** derivative of weight loss versus temperature.

temperature at the maximum weight loss rate (T_{max}) and lower char residue.

As epoxy vol% increased in the epoxy/solvent solution, the degradation temperature at the maximum weight loss rate of CNF/epoxy nanocomposite foam samples also increased. All the samples had a higher temperature at the maximum weight loss rate than the neat epoxy sample. For example, both (T_{max}) of CNF/EPT40 and CNF/EPE40 increased by 33.0 °C as compared to neat epoxy resin. This could be attributed to the interlocking of CNF with epoxy resin which required additional energy to degrade the nanocomposites. Moreover, it is possible that the porous structure influenced thermal transfer through the whole sample to improve the thermal stability. The CNF/epoxy nanocomposite foam samples from higher epoxy volume content had lower char residue. Because the char residue was primarily contributed by the CNF aerogel, compared to CNF weight, the epoxy in the CNF/EP samples was higher weight percent. So the char residue of CNF/EP samples decreased as epoxy content increased. The char residue of CNF aerogel at 650 °C was 6 times higher than the neat epoxy sample at 4.3%. Compared with the CNF/epoxy nanocomposites fabricated with THF solvent and EA solvent, the trends and maximum weight loss rate of samples fabricated with different volume contents of epoxy/EA solution were more concentrated than the samples fabricated with different ratio of epoxy/THF solution. This may be caused by the dispersion of epoxy/solvent solution. The THF solvent was observed to have had better dispersion in epoxy resin, which made more uniform structures for the CNF/epoxy nanocomposite foams, Fig. 2. It could be concluded that the thermal stability of nanocomposites varied with formulations and solvent used to dissolve the epoxy resin.

The glass transition temperature (T_g) of neat epoxy and nanocomposites was measured by DSC, as shown in Table 3. The overall finding was that the presence of CNF increased the T_g as compared to neat epoxy, and this effect was even more pronounced for sample CNF/EPE10, CNF/EPE/20, and all nanocomposites prepared from THF. The CNF/EPE30 and CNF/EPE40 nanocomposites showed lower T_g than that of CNF/EPE10 and CNF/EPE20, suggesting that impregnation of CNF foam in epoxy/EA solution did not reach saturation level for CNF/EPE30 and CNF/EPE40. Although highest density value was observed for CNF/EPT40 nanocomposites,

Table 3 T_g for each sample determined by DSC

Sample	T_g (°C)[a]
Epoxy	47.2
CNF/EPT10	56.9
CNF/EPT20	54.8
CNF/EPT30	54.8
CNF/EPT40	54.6
CNF/EPE10	57.1
CNF/EPE20	58.4
CNF/EPE30	53.7
CNF/EPE40	50.4

[a]Difference between duplicates is less than 0.1%, so the standard derivation is not added

indicating the highest amount of epoxy was infused into CNF foam, the T_g did not change with increased epoxy concentration in THF from 10 to 40%. This was attributed to the porous structure of CNF foam, which may result in enhanced mechanical interlocking/interaction with the epoxy polymer chains. Hence, when the fraction of epoxy increased from CNF/EPT20 to CNF/EPT40, the T_g increased accordingly because interlocking capacity of the specific amount of CNF was already fully capture in CNF/EPT20. These phenomena suggest the diffusion of epoxy resin in THF into CNF foam is more efficient, while higher concentration of epoxy in EA solvent is required to reach to an equivalent fraction of epoxy in the final nanocomposites.

Water absorption

CNF/epoxy nanocomposites were immersed in DI water for 24 h. The absolute water absorption (WA) curves were plotted, Fig. 6, initially every 1 h up to 4 h then every 4 h after to show percent weight gain as a function of time after 24 h immersion in water. The pure CNF foam dissolved quickly in DI water, and the neat cured epoxy resin was water insoluble material; thus, both of samples were not reported in Fig. 6. The results show that the WAs of CNF/epoxy samples fabricated using epoxy with THF or EA solutions decreased with increased epoxy loading. Both CNF/EPT10 and CNF/EPE10 samples had the highest WA of 1016.7 and 914.4%, followed by samples with epoxy loading of 20, 30 and 40 vol% in either THF solvent or EA solvent, respectively. The values of apparent porosity and apparent water/sample volume ratio for CNF/epoxy samples with
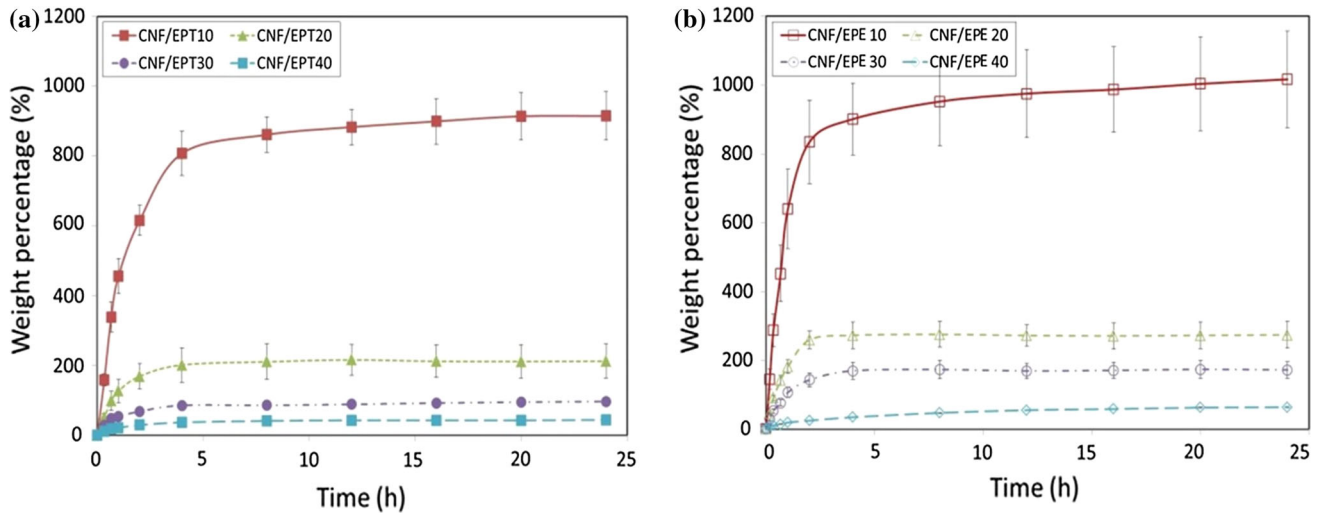
Figure 6 Water absorption of THF samples and EA samples with different percentage of epoxy.

different formulas are shown in Table 4. The apparent porosity was calculated based on the weight of samples, the density of solid raw materials (cellulose: 1.5 g/cm^3 and epoxy: 1.1 g/cm^3) and pure CNF aerogel density (0.013 g/cm^3). The results showed that the porosity decreased with an increase in epoxy loading, as expected. The water/sample volume ratio was calculated by the final absorbed water and sample dimension. The results showed that the water/sample volume ratio was increased for the samples with higher porosity. The free water was absorbed into the porous sample. However, the results also showed that the porosity was not completely occupied by the water. The porous size could affect the water absorption behavior of the samples.

Further, the EA samples had higher water absorption than the THF samples in the same epoxy loading level. Because the THF solvent might have better dispersion and compatibility for epoxy resin by

the observation, the epoxy had better coverage of CNF surface than the samples fabricated by epoxy/EA solution. The EA solvent dissolved epoxy resin, but the solubility of the epoxy resin in EA was poorer than in THF, as indicated by morphological and density results (Figs. 3, 4). Furthermore, water absorption rates of the CNF/epoxy nanocomposite foams were determined using Fick's law of diffusion model by water absorbed (MC) versus time 1/2 with a polynomial curve fitting using a second-order equation fit [31]. The diffusion coefficient D_f for CNF/EPT and CNF/EPE samples from 10 to 40% by vol% were 157.7, 52.9, 20.9, 7.2 and 278.3, 83.2, 45.8, 3.9, respectively (Table 4). Results show the water absorption rate increased with a decreased amount of epoxy loading. The epoxy concentration was a major factor causing differences in water absorption value. Samples exhibiting higher water absorption had higher diffusion coefficients. In the future, it may be

Table 4 Diffusion coefficient of each sample

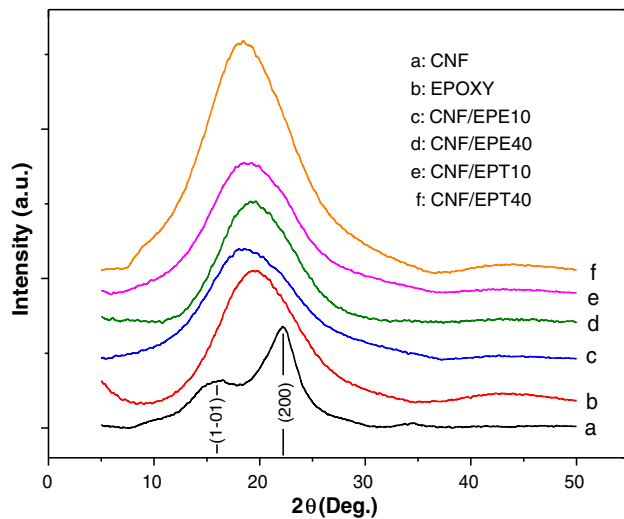| Sample	Porous percentage (%)	Water/sample volume ratio (%)	Diffusion coefficient (10^{-6} m^2/s)
CNF/EPT10	96.2	44.9	157.7
CNF/EPT20	84.6	39.6	52.9
CNF/EPT30	69.2	35.3	20.9
CNF/EPT40	31.9	30.8	7.2
CNF/EPE10	95.1	51.8	278.3
CNF/EPE20	85.4	43.3	83.2
CNF/EPE30	79.5	38.2	45.8
CNF/EPE40	53.6	33.2	7.9

Figure 7 XRD patterns of CNF, neat epoxy and nanocomposites.

desired to incorporate water absorption characteristics that could be designed based on the CNF/epoxy formulas for the different applications.

Crystalline structures

Wide angle XRD was used to determine the effect of CNF on the macro- and microstructure changes of epoxy based nanocomposites. Figure 7 shows the XRD patterns of CNF, epoxy, and nanocomposites. The CNF exhibits two peaks at 16.4° and 22.5°, corresponding to diffractions planes (1-01) and (110), respectively [35]. In the case of neat epoxy, a wide diffraction from 10° to 35° was caused by scattering of the cured epoxy molecules, indicating its amorphous nature [36]. Note that all CNF/epoxy nanocomposites showed similar diffraction patterns as the neat epoxy. The two characteristic diffraction peaks of CNF disappeared in the nanocomposites, demonstrating the relatively low weight fraction of CNF was well encapsulated by epoxy. Furthermore, the results suggested the crystalline structure of epoxy resin was not influenced by compounding with CNF.

Conclusions

In this paper, CNF/epoxy nanocomposite foam with a cross-linked structure and alterable properties has been developed using CNF aerogel and epoxy diluted solutions. Both diluted epoxy/tetrahydrofuran (THF) solutions and epoxy/ethyl acetate (EA) solutions with different concentrations were infused into

CNF aerogels to improve their compressive performance and stability for potential use in structural materials.

The microstructure and surface morphology of CNF/epoxy composite foams observed with scanning electron microscope showed that CNF crosslinked fibers were well encapsulated by epoxy resin after solvent volatilization. The CNF flake-like microwalls were swollen after the epoxy infusing process at lower epoxy loading. Moreover, as epoxy vol% increased it was observed in the SEM micrographs there was a less porous structure at the 30 and 40 vol% epoxy loading. The concentration of epoxy/solvent solution in both THF and EA solvents was shown to have a significant effect on the compressive properties. The samples fabricated with higher epoxy loading had higher compressive properties. The CNF/epoxy nanocomposite foam fabricated by the epoxy/THF solution had higher density and better performance than foam fabricated by epoxy/EA solution due to improved solubility and dispersion. Water resistance of CNF/epoxy composites foams with low epoxy loading had higher water absorption. The CNF/epoxy composites foams fabricated by the epoxy/THF solution had lower water absorption than foams fabricated by epoxy/EA solution at the same loading level. Because the porous structure affected the water absorption behavior, more porous structure in the sample with less epoxy loading had larger spaces for the free water, resulting in higher absorptions. The thermal stability of CNF/epoxy nanocomposite foam results showed CNF/EP nanocomposite foam had higher degradation temperature than the pure CNF aerogel and neat epoxy samples. The porous structure resisted the thermal transfer and improved the thermal stability. The T_g was determined by differential scanning calorimetry. T_g of the nanocomposites was influenced by the CNF/epoxy composition. Therefore, it is possible to engineer a CNF/epoxy nanocomposite foam having significantly different physical and mechanical properties and possible to optimize via changing the concentration of epoxy resin in solvent.

Acknowledgements

the support of James Bridwell of EMRSL group for the mechanical testing.

Compliance with ethical standards

References

[1] Fowler PA, Hughes JM, Elias RM (2006) Biocomposites: technology, environmental credentials and market forces. J Sci Food Agric 86:1781–1789

[2] Zhang J, Luo N, Zhang X, Xu L, Wu J, Yu J et al (2016) All-cellulose nanocomposites reinforced with in situ retained cellulose nanocrystals during selective dissolution of cellulose in an ionic liquid. ACS Sustain Chem Eng 4:4417–4423

[3] Huber T, Müssig J, Curnow O, Pang S, Bickerton S, Staiger MP (2012) A critical review of all-cellulose composites. J Mater Sci 47:1171–1186. doi:10.1007/s10853-011-5774-3

[4] Lee S-Y, Chun S-J, Kang I-A, Park J-Y (2009) Preparation of cellulose nanofibrils by high-pressure homogenizer and cellulose-based composite films. J Ind Eng Chem 15:50–55

[5] Khalil HPSA, Bhat AH, Yusra AFI (2012) Green composites from sustainable cellulose nanofibrils: a review. Carbohydr Polym 87:963–979

[6] Jeronimidis G (1980) Wood, one of nature's challenging composites. Symp Soc Exp Biol 34:169–182

[7] Bledzki AK, Gassan J (1999) Composites reinforced with cellulose based fibres. Prog Polym Sci 24:221–274

[8] Gebald C, Wurzbacher JA, Tingaut P, Zimmermann T, Steinfeld A (2011) Amine-based nanofibrillated cellulose as adsorbent for CO_2 capture from air. Environ Sci Technol 45:9101–9108

[9] Zhang Z, Sèbe G, Rentsch D, Zimmermann T, Tingaut P (2014) Ultralightweight and flexible silylated nanocellulose sponges for the selective removal of oil from water. Chem Mater 26:2659–2668

[10] Yao C, Hernandez A, Yu Y, Cai Z, Wang X (2016) Triboelectric nanogenerators and power-boards from cellulose nanofibrils and recycled materials. Nano Energy 30:103–108

[11] Chen B, Zheng Q, Zhu J, Li J, Cai Z, Chen L et al (2016) Mechanically strong fully biobased anisotropic cellulose aerogels. RSC Adv 6:96518–96526

[12] Jung YH, Chang T-H, Zhang H, Yao C, Zheng Q, Yang VW et al (2015) High-performance green flexible electronics based on biodegradable cellulose nanofibril paper. Nat Commun 6:7170

[13] Zheng Q, Javadi A, Sabo R, Cai Z, Gong S (2013) Polyvinyl alcohol (PVA)–cellulose nanofibril (CNF)–multiwalled carbon nanotube (MWCNT) hybrid organic aerogels with superior mechanical properties. RSC Adv 3:20816–20823

[14] Yao C, Wang F, Cai Z, Wang X (2016) Aldehyde-functionalized porous nanocellulose for effective removal of heavy metal ions from aqueous solutions. RSC Adv 6:92648–92654

[15] Lee Y, Choi J-W, Suh DJ, Ha J-M, Lee C-H (2015) Ketonization of hexanoic acid to diesel-blendable 6-undecanone on the stable zirconia aerogel catalyst. Appl Catal A 506:288–293

[16] Buratti C, Moretti E, Belloni E, Agosti F (2014) Development of innovative aerogel based plasters: preliminary thermal and acoustic performance evaluation. Sustainability 6:5839–5852

[17] Li Z, Yao C, Wang F, Cai Z, Wang X (2014) Cellulose nanofiber-templated three-dimension TiO_2 hierarchical nanowire network for photoelectrochemical photoanode. Nanotechnology 25:504005

[18] Zheng Q, Cai Z, Ma Z, Gong S (2015) Cellulose nanofibril/reduced graphene oxide/carbon nanotube hybrid aerogels for highly flexible and all-solid-state supercapacitors. ACS Appl Mater Interfaces 7:3263–3271

[19] Zheng Q, Cai Z, Gong S (2014) Green synthesis of polyvinyl alcohol (PVA)–cellulose nanofibril (CNF) hybrid aerogels and their use as superabsorbents. J Mater Chem A 2:3110–3118

[20] Hodgkin JH, Simon GP, Varley RJ (1998) Thermoplastic toughening of epoxy resins: a critical review. Polym Adv Technol 9:3–10

[21] Li J, Hunt JF, Cai Z, Zhou X (2013) Bending analyses for 3D engineered structural panels made from laminated paper and carbon fabric. Compos Part B Eng 53:17–24

[22] Li J, Hunt JF, Gong S, Cai Z (2016) Simplified analytical model and balanced design approach for light-weight wood-based structural panel in bending. Compos Struct 136:16–24

[23] Li J, Hunt JF, Gong S, Cai Z (2016) Fatigue behavior of wood-fiber-based tri-axial engineered sandwich composite panels (ESCP). Holzforschung 70:567–575

[24] Li J, Hunt JF, Gong S, Cai Z (2015) Testing and evaluation of a slot and tab construction technique for light-weight wood-fiber-based structural panels under bending. J Test Eval 44:357–366

[25] Li J, Hunt JF, Gong S, Cai Z (2014) High strength wood-based sandwich panels reinforced with fiberglass and foam. BioResources 9:1898–1913

[26] Saito T, Hirota M, Tamura N, Kimura S, Fukuzumi H, Heux L et al (2009) Individualization of nano-sized plant cellulose fibrils by direct surface carboxylation using TEMPO catalyst under neutral conditions. Biomacromolecules 10:1992–1996

[27] Qing Y, Sabo R, Zhu J, Agarwal U, Cai Z, Wu Y (2013) A comparative study of cellulose nanofibrils disintegrated via

multiple processing approaches. Carbohydr Polym 97:226–234

[28] Standard A (2010) D695, 2010 standard test method for compressive properties of rigid plastics. ASTM International, West Conshohocken

[29] Wei L, Liang S, McDonald AG (2015) Thermophysical properties and biodegradation behavior of green composites made from polyhydroxybutyrate and potato peel waste fermentation residue. Ind Crops Prod 69:91–103

[30] Standard A (1998) D570-98: standard test method for water absorption of plastics. American Society for Testing and Materials, New York

[31] Wei L, McDonald AG, Freitag C, Morrell JJ (2013) Effects of wood fiber esterification on properties, weatherability and biodurability of wood plastic composites. Polym Degrad Stab 98:1348–1361

[32] Mueller S, Sapkota J, Nicharat A, Zimmermann T, Tingaut P, Weder C et al (2015) Influence of the nanofiber dimensions on the properties of nanocellulose/poly (vinyl alcohol) aerogels. J Appl Polym Sci 132:13

[33] Kumar A, Negi YS, Choudhary V, Bhardwaj NK (2014) Characterization of cellulose nanocrystals produced by acid-hydrolysis from sugarcane bagasse as agro-waste. J Mater Phys Chem 2:1–8

[34] Soni B, Mahmoud B (2015) Chemical isolation and characterization of different cellulose nanofibers from cotton stalks. Carbohydr Polym 134:581–589

[35] Xu X, Liu F, Jiang L, Zhu J, Haagenson D, Wiesenborn DP (2013) Cellulose nanocrystals vs. cellulose nanofibrils: a comparative study on their microstructures and effects as polymer reinforcing agents. ACS Appl Mater Interfaces 5:2999–3009

[36] Wan Y-J, Gong L-X, Tang L-C, Wu L-B, Jiang J-X (2014) Mechanical properties of epoxy composites filled with silane-functionalized graphene oxide. Compos Part A Appl Sci Manuf 64:79–89